Inhibition of AmpC β-Lactamase through a Destabilizing Interaction in the Active Site[†,‡]

Indi Trehan,[§] Beth M. Beadle,[§] and Brian K. Shoichet*

Department of Molecular Pharmacology and Biological Chemistry, Northwestern University Medical School, Northwestern University, 303 East Chicago Avenue, Chicago, Illinois 60611-3008

Received March 30, 2001; Revised Manuscript Received May 11, 2001

ABSTRACT: β-Lactamases hydrolyze β-lactam antibiotics, including penicillins and cephalosporins; these enzymes are the most widespread resistance mechanism to these drugs and pose a growing threat to public health. β-Lactams that contain a bulky 6(7)α substituent, such as imipenem and moxalactam, actually inhibit serine β-lactamases and are widely used for this reason. Although mutant serine β-lactamases have arisen that hydrolyze β-lactamase resistant β-lactams (e.g., ceftazidime) or avoid mechanism-based inhibitors (e.g., clavulanate), mutant serine β-lactamases have not yet arisen in the clinic with imipenemase or moxalactamase activity. Structural and thermodynamic studies suggest that the 6(7)α substituents of these inhibitors form destabilizing contacts within the covalent adduct with the conserved Asn152 in class C β-lactamases (Asn132 in class A β-lactamases). This unfavorable interaction may be crucial to inhibition. To test this destabilization hypothesis, we replaced Asn152 with Ala in the class C β-lactamase AmpC from *Escherichia coli* and examined the mutant enzyme's thermodynamic stability in complex with imipenem and moxalactam. Consistent with the hypothesis, the Asn152 → Ala substitution relieved 0.44 and 1.10 kcal/mol of strain introduced by imipenem and moxalactam, respectively, relative to the wild-type complexes. However, the kinetic efficiency of AmpC N152A was reduced by 6300-fold relative to that of the wild-type enzyme. To further investigate the inhibitor's interaction with the mutant enzyme, the X-ray crystal structure of moxalactam in complex with N152A was determined to a resolution of 1.83 Å. Moxalactam in the mutant complex is significantly displaced from its orientation in the wild-type complex; however, moxalactam does *not* adopt an orientation that would restore competence for hydrolysis. Although Asn152 forces β-lactams with 6(7)α substituents out of a catalytically competent configuration, making them inhibitors, the residue is essential for orienting β-lactam substrates and cannot simply be replaced with a much smaller residue to restore catalytic activity. Designing β-lactam inhibitors that interact unfavorably with this conserved residue when in the covalent adduct merits further investigation.

β-Lactamase expression is the most prevalent mechanism of bacterial resistance to the β-lactam family of antibiotics, which includes the penicillins and cephalosporins (*1*). Their occurrence in many bacterial pathogens poses a threat to public health (*2*−*4*) and a challenge to medicinal chemists when developing new and more effective β-lactam antibiotics. Class C β-lactamases, such as AmpC, are especially important among Gram-negative nosocomial pathogens. The mechanism of AmpC (Figure 1) involves a catalytic serine (Ser64) that acts as a nucleophile and attacks the carbonyl carbon of the β-lactam ring, rapidly forming an acyl−enzyme complex with the β-lactam. This reaction resembles that of serine proteases (*5*). The deacylation of this covalent enzyme−ligand intermediate complex typically proceeds more slowly; a water molecule attacks the same carbon and hydrolyzes the serine ester, forming the product of the

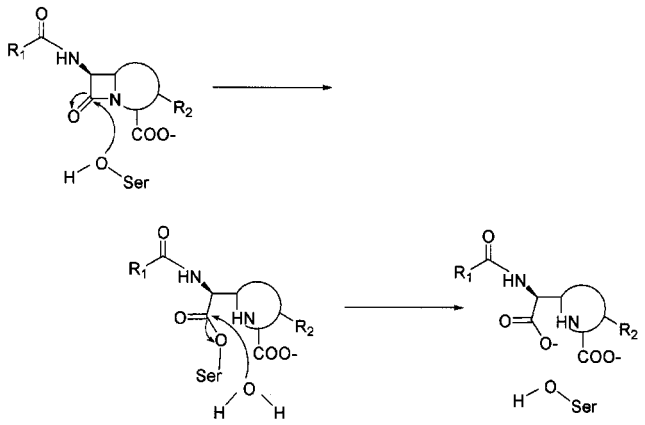

FIGURE 1: Simplified mechanism of serine β-lactamases. In the first step, the catalytic serine (Ser64 in class C and Ser70 in class A) attacks the carbonyl carbon of the β-lactam ring, forming an acyl intermediate. In the second step, a deacylating water hydrolyzes the ester bond to regenerate the enzyme and the reaction product, hydrolyzed antibiotic. The deacylation step is generally slower with β-lactam-based inhibitors.

[†] Supported by NSF Grant MCB-9734484 (to B.K.S.). I.T. is a Howard Hughes Medical Institute Medical Student Research Training Fellow. B.M.B. is partly supported by NIH Grant T32-GM08382.

[‡] The coordinates for the N152A mutant AmpC structure in complex with moxalactam have been deposited in the Protein Data Bank as entry 1I5Q.

* To whom correspondence should be addressed: Department of Molecular Pharmacology and Biological Chemistry, Mail Code S215, 303 E. Chicago Ave., Chicago, IL 60611-3008. E-mail: b-shoichet@northwestern.edu. Telephone: (312) 503-0081. Fax: (312) 503-5349.

[§] These authors contributed equally to this work.

10.1021/bi010641m CCC: $20.00
Published on Web 06/13/2001

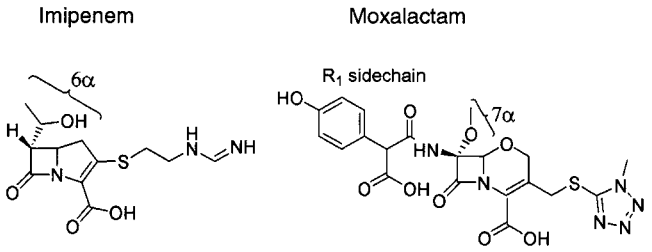

FIGURE 2: Structures of the β-lactamase inhibitors imipenem and moxalactam.

reaction and restoring the free enzyme. Seemingly subtle differences in the structures of β-lactams can convert an excellent substrate into a molecule whose deacylation is so slow that it effectively acts as an inhibitor. Such inhibitors, or "β-lactamase resistant" β-lactams, retain their efficacy against many resistant bacteria expressing serine β-lactamases. Recently, several new β-lactamases have arisen that hydrolyze these inhibitory β-lactams (*6*−*8*), raising renewed fears of β-lactam resistance. Both the mechanisms of inhibition of, and the origins of resistance to, β-lactams have been intensely studied (*9*−*20*).

With new patterns of resistance emerging, drugs such as imipenem and moxalactam are widely used because they have retained their ability to inhibit or resist most serine β-lactamases. In these molecules, a relatively bulky group has replaced the proton that typically occupies the 6(7)α position on the β-lactam ring (*21*) (Figure 2). Crystal structures of imipenem bound to the class A β-lactamase TEM-1 (*16*) and of moxalactam bound to the class C β-lactamase AmpC (*19*) suggest that bulky 6(7)α groups make unfavorable contacts with the conserved Asn152 in AmpC (Asn132 in TEM-1). These close contacts force the inhibitors to adopt unusual, strained conformations in the active site that do not allow for hydrolytic attack of the acyl−enzyme complex. Consistent with this view, both imipenem and moxalactam actually destabilize AmpC in their covalent complexes with the enzyme, whereas β-lactams such as cloxacillin and aztreonam, which lack bulky 6(7)α substituents, stabilize AmpC (*22*). This destabilization reflects unfavorable noncovalent interactions within the covalent imipenem and moxalactam adducts and may be largely due to high-energy contacts with the conserved Asn152 (Asn132) that are observed crystallographically.

If unfavorable interactions with Asn152 are crucial to β-lactamase inhibition by moxalactam and imipenem, it is reasonable to wonder why β-lactamases such as AmpC and TEM-1 have not simply evolved site substitutions that replace Asn152 (Asn132) (*23*), relieving the strain introduced by the inhibitors and thereby allowing them to be hydrolyzed. Of the more than 90 clinically isolated mutants of TEM-1, not one has involved a substitution of Asn132, nor have any shown activity against imipenem or moxalactam. This might suggest either that Asn132 (Asn152) is not, in fact, involved in destabilizing interactions with moxalactam and imipenem or that this residue is functionally important and cannot be replaced. The latter explanation would be consistent with mutagenesis studies in AmpC (*24*) that suggest that substitutions to Asn152 dramatically reduce the activity of the enzyme (*25*).

To investigate the importance of Asn152 in destabilization and inhibition of AmpC by β-lactams containing 6(7)α substituents, we have made the mutant AmpC N152A[1] and determined the effect of moxalactam and imipenem on its stability. If the destabilizing effects of moxalactam and imipenem are a result of van der Waals violations with Asn152, as we hypothesize, the Asn152 → Ala substitution should result in complexes that are stabilized relative to the WT complexes. To explore why this substitution has not arisen in nature, we have investigated the effect of this substitution on the catalytic efficiency of the enzyme and have determined the structure of N152A in complex with moxalactam by X-ray crystallography.

MATERIALS AND METHODS

Enzyme Preparation. The mutant AmpC N152A was prepared from the wild-type ampC gene in the plasmid pOGO295 using the overlap extension polymerase chain reaction (*26*). This plasmid confers tetracycline resistance and contains a temperature-sensitive repressor that controls the expression of the ampC gene. Following mutagenesis, the mutant plasmid was transformed back into *Escherichia coli* JM109 cells for expression.

Expression of AmpC N152A was performed as described previously (*17*), with slight modifications. A 2 L fermenter was charged with 2 L of 2×YT broth (Fisher, Fair Lawn, NJ), 2 mL of 10 mg/mL tetracycline hydrochloride, and 25 mL of an overnight culture of *E. coli* JM109 cells transformed with the mutant plasmid. The culture was grown at 37 °C, with 400 rpm agitation and 2 L/min of air flow, until the OD_{600} reached 0.3−0.5. At this time, the temperature of the culture was increased to 40.8 °C, and the culture was left under these conditions for 18−24 h. After this time, the air flow was reduced to 1 L/min for 2−4 h. Following this, the mutant enzyme was isolated and purified as described previously (*19*).

CD Measurements. Thermal denaturation experiments were carried out in a Jasco J-715 spectropolarimeter with a Jasco PTC-348WI Peltier-effect temperature control device and in-cell stirring. N152A was denatured in buffer composed of 50 mM potassium phosphate (KP_i), 200 mM potassium chloride (KCl), and 38% (v/v) ethylene glycol, at pH 6.8, as described previously (*22*). The far-UV region at 223 or 232 nm was used for monitoring secondary structure motifs (although the 232 nm wavelength monitors the edge of the helical CD signal, it is less affected by absorbance from β-lactams; the two wavelengths return equivalent thermodynamic results). Thermal melts were performed at temperature ramp rates of 2 K/min. A least-squares fit of the two-state transition model was performed by the EXAM software program (*27*) to calculate T_m and ΔH_{VH} for the thermal denaturations. The ΔC_p was set to 6.0 kcal mol^{-1} K^{-1}. Prior work (*22*) has demonstrated that AmpC denaturation is consistent with a two-state, reversible model, and our results here are also consistent with such a model.

Denaturation of N152A alone was carried out by adding 6 μL of the enzyme solution (6.9 mg/mL) to 3.5 mL of the buffer solution. Denaturation experiments with enzyme−

[1] Abbreviations: WT, wild-type; N152A, mutant form of AmpC (alanine substituted for asparagine 152); T_m, temperature of melting; ΔC_p, change in heat capacity at constant pressure; k_{cat}, catalytic rate constant; K_M, Michaelis−Menten constant; ΔH_{VH}, van't Hoff enthalpy; $\Delta\Delta G_u$, change in Gibbs free energy of unfolding.

Table 1: Thermodynamic Denaturation Data for WT and N152A Apo AmpC in Complex with Moxalactam and Imipenem

	T_m (°C)	ΔH_{VH} (kcal/mol)	ΔT_m (°C)	$\Delta\Delta G_u$ (kcal/mol)
WT apo[a]	54.6 ± 0.2	182 ± 9	–	–
WT and imipenem[a]	53.4 ± 0.1	156 ± 6	−1.2 ± 0.2	−0.7 ± 0.1
WT and moxalactam[a]	51.4 ± 0.1	200 ± 15	−3.2 ± 0.2	−1.8 ± 0.1
N152A apo	52.0 ± 0.2	184 ± 12	–	–
N152A and imipenem	51.6 ± 0.2	157 ± 7	−0.4 ± 0.3	−0.2 ± 0.2
N152A and moxalactam	50.8 ± 0.3	209 ± 20	−1.2 ± 0.4	−0.7 ± 0.2

[a] From Beadle et al. (*22*).

Table 2: Data Collection and Refinement Statistics

space group	*C*2
unit cell dimension	*a* = 117.66 Å *b* = 77.27 Å *c* = 97.68 Å *β* = 116.76°
no. of complexes per asymmetric unit	2
resolution (Å)	1.83
no. of observed reflections	274720
no. of unique reflections	68795
completeness (%)[a]	99.8 (99.9)
R_{merge} (%)[a]	5.1 (40.9)
$\langle I/\sigma_I \rangle$	22.08
no. of working reflections	57575
resolution range for refinement (Å)[a]	20.0−1.83 (1.87−1.83)
no. of protein residues	714
no. of protein atoms in the final model	5580
no. of non-hydrogen ligand atoms	58
no. of water molecules	394
rmsd for bond lengths (Å)	0.0139
rmsd for bond angles (deg)	1.72
R_{cryst} (%)	16.8
R_{free} (%)[b]	20.6
average *B*-factor (Å^2)	
protein	28.73[c]
protein (monomer 2)	27.85
ligand	40.62[c]
ligand (monomer 2)	35.94
solvent	38.56[c]

[a] Values in parentheses are for the highest-resolution shell used in refinement. [b] R_{free} was calculated with 3% of the reflections set aside randomly. [c] Values cited were calculated for both molecules in the asymmetric unit.

ligand complexes were carried out by preincubating N152A with ligand (72-fold excess). For moxalactam (Sigma, St. Louis, MO), a maximum ΔT_m was reached within 45 min and sustained for at least 20 h. For imipenem (Merck, Whitehouse Station, NJ), the ΔT_m measured immediately following incubation is reported here. Following incubation, 20 μL of the enzyme−ligand solution was added to 3.5 mL of pre-equilibrated buffer solution, and denaturation was performed as with the enzyme alone. Each denaturation experiment was performed at least in triplicate. $\Delta\Delta G_u$ values were computed from ΔT_m measurements using the method of Schellman (*29*), as described previously (*22*).

Kinetic Assays. The activity of N152A was assayed by its hydrolysis of the characteristic β-lactam substrate cephalothin (Sigma) (*30*−*32*). The reaction buffer used in these experiments was 50 mM KP_i and 50 mM KCl, at pH 7.0 (*33*). The k_{cat} and K_M values for N152A were determined at an enzyme concentration of 3 μM; the initial concentration of cephalothin ranged from 200 to 2000 μM. The reactions were performed in 0.1 cm path length quartz cells (Hellma Cells, Jamaica, NY) and were monitored at a wavelength of 265 nm.

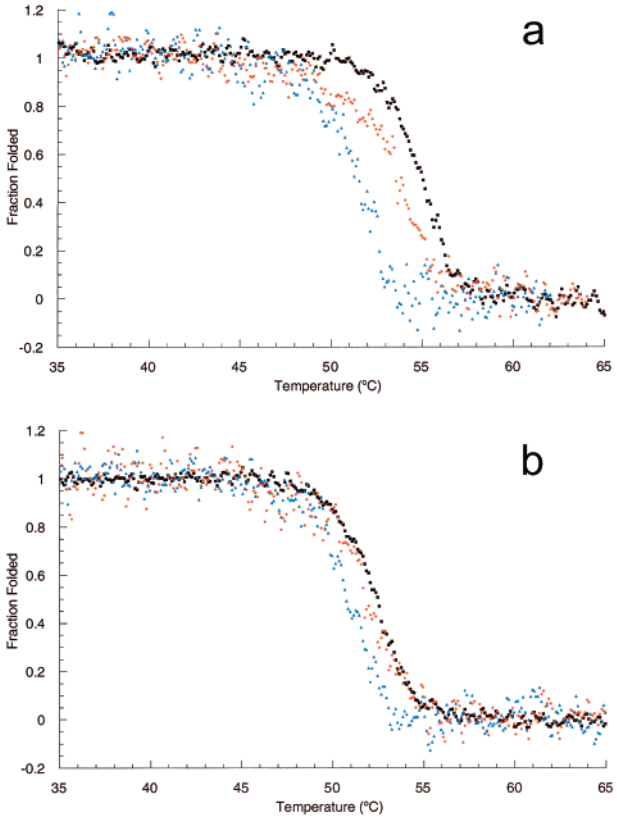

FIGURE 3: Reversible, apparently two-state thermal denaturation curves of (a) AmpC WT and (b) AmpC N152A. Black squares represent the apoenzyme, red diamonds the enzyme in complex with imipenem, and blue triangles the enzyme in complex with moxalactam. Data points represent a pairwise moving average between adjacent measurements.

Crystal Growth. N152A crystals were grown by vapor diffusion in hanging drops over a solution of 1.7 M KP_i at pH 8.7 and 23 °C, after microseeding with the wild-type enzyme. A 6 μL drop of N152A at an initial concentration of 98 μM in 1 M KP_i (pH 8.7) was placed on a cover slip. To this drop was added 1 μL of the seed solution (0.2 mm crystal crushed in 44 μL of 1.7 M KP_i, at pH 8.7). Serial dilution transfers of 1 μL each were then carried out across five more hanging drops (each containing 6 μL of the N152A solution). Crystals appeared in 5−7 days.

After retrieval, N152A crystals were soaked in excess (approximately 50 mM) moxalactam solution in crystallizing buffer for 1.5 h. Before being flash-frozen in liquid nitrogen, crystals were cryoprotected in a solution containing 20% sucrose, 1.7 M KP_i, and 50 mM moxalactam, at pH 8.7.

Data Collection and Processing. X-ray diffraction data were collected at DND-CAT beamline 5IDB at the Advanced Photon Source at Argonne National Laboratory (Argonne, IL) at 100 K using a 162 mm Mar CCD detector. The reflections were indexed, integrated, and scaled using the HKL software suite (*34*) (Table 2). AmpC crystallizes in the *C*2 space group, with two AmpC molecules in the asymmetric unit, each containing 358 amino acid residues. Three percent of the reflections, chosen at random, were set aside as the test set. The initial model was built by molecular replacement using an AmpC−boronic acid complexed structure (*18*), with inhibitor and solvent atoms removed and Asn152 replaced with Ala. After the phases were calculated, the model was subjected to rigid body, simulated annealing,

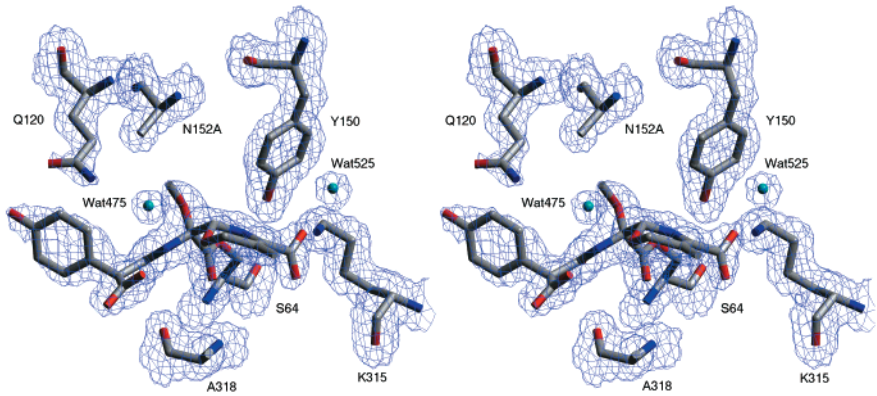

FIGURE 4: Stereoview of $2|F_o| - |F_c|$ electron density of the refined model of AmpC N152A in complex with moxalactam, contoured at 1σ. The active site region from molecule 2 of the asymmetric unit is shown here and in all subsequent figures, with moxalactam covalently bound to Ser64. Carbon atoms are colored gray, oxygen atoms red, and nitrogen atoms blue. Ordered water molecules are depicted as cyan-colored spheres. This figure was generated using SETOR (*51*).

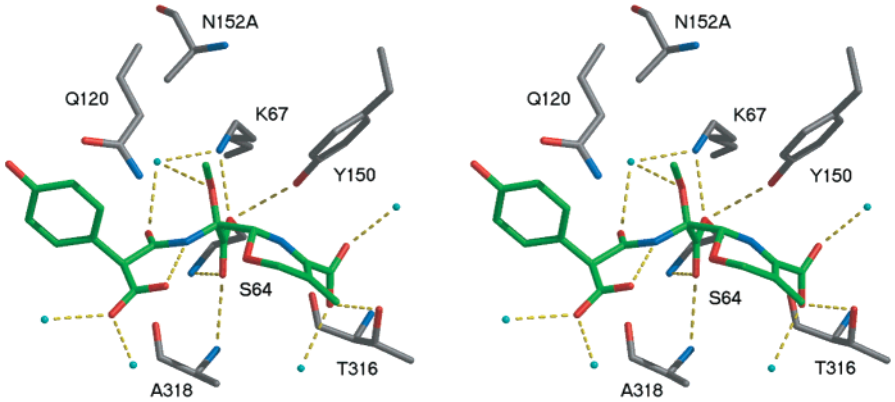

FIGURE 5: Stereoview of the active site of AmpC N152A covalently bound to moxalactam. Atoms are colored as described in the legend of Figure 4, except moxalactam carbon atoms are colored green. Dashed yellow lines represent hydrogen bond interactions. This figure was generated using MidasPlus (*52*).

positional minimization, and individual *B*-factor refinement using the CNS software package (*35*). The maximum likelihood target was used during refinement, including a bulk solvent correction and a 2σ cutoff. Sigma-A weighted electron density maps were generated in CNS. Manual model building was performed using O (*36*), alternating with rounds of positional and individual *B*-factor refinement in CNS. The stereochemical quality of the model was monitored periodically with the program Procheck (*37*).

Poor electron density was noted for residues 280−291 in molecule 1 of the asymmetric unit, and several residues were modeled at half-occupancy to reflect this. Further, residues 282 and 284 and the side chain of residue 286 of molecule 1 were excluded from the model due to this poor density. In general, molecule 2 of the asymmetric unit exhibited stronger electron density in both active and non-active site regions of the protein. Moxalactam was built into the $2|F_o| - |F_c|$ and $|F_o| - |F_c|$ difference density in both molecules in the asymmetric unit and modeled in at full occupancy.

RESULTS

Thermal Denaturation of N152A Complexes. To investigate how the side chain of Asn152 contributes to the interaction of moxalactam and imipenem with AmpC, the mutant enzyme N152A was thermally denatured alone and in complex with moxalactam or imipenem. Compared to the apo form of AmpC N152A, the moxalactam adduct was destabilized by 1.2 °C, equivalent to a decrease in stability of 0.7 kcal/mol (Figure 3 and Table 1). This is significantly lower than the 1.8 kcal/mol destabilization of WT AmpC by moxalactam. The imipenem adduct was destabilized by 0.4 °C after incubation for 5 min, equivalent to a decrease in stability of 0.2 kcal/mol (Figure 3 and Table 1). This, too, is significantly lower than the 0.7 kcal/mol destabilization of WT when complexed with imipenem. The strain introduced by imipenem and moxalactam was thus relieved in N152A by 0.44 and 1.10 kcal/mol, respectively, relative to their interactions with the wild-type enzyme (Table 1).

Kinetic Analysis of AmpC N152A. The hydrolysis of the β-lactam substrate cephalothin was monitored by UV−vis spectroscopy (*31*, *33*). Background rates of cephalothin hydrolysis in buffer alone were also measured; these rates were negligible compared to the rate of N152A-catalyzed hydrolysis. The k_{cat} and K_M values for AmpC N152A were 1.3 s^{-1} and 1600 μM, respectively. The k_{cat}/K_M value was 0.79 mM^{-1} s^{-1}, 6300 times lower than that of WT AmpC, consistent with previously reported values (*24*).

Crystal Structure of AmpC N152A in Complex with Moxalactam. To understand structurally how the mutant enzyme interacts with a β-lactam bearing a 6(7)α substituent, the X-ray crystal structure of moxalactam bound to N152A was determined to a resolution of 1.83 Å (Table 2). The electron density for the inhibitor was well-defined in both molecules of the asymmetric unit, particularly in molecule

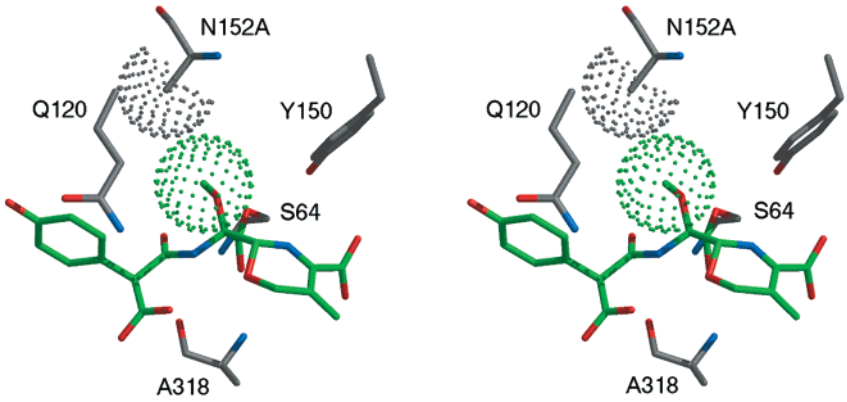

FIGURE 6: Stereoview of van der Waals radii of the 7α-methoxy group of moxalactam and Cβ of Ala152 of AmpC N152A. Atoms are colored as described in the legend of Figure 5. In contrast to the overlapping interaction seen in the wild-type form of AmpC in complex with moxalactam (*19*), this mutant form of the enzyme shows no steric clash due to van der Waals overlap. This figure was generated using MidasPlus (*52*).

2 (Figure 4). The quality of the final model was evaluated with Procheck (*37*): 92.6% of the amino acid residues were in the most favored regions of the Ramachandran plot, and the remaining 7.4% were in additionally allowed regions, excluding proline and glycine residues. The final R_{cryst} and R_{free} values of the refined structure were 16.8 and 20.6%, respectively. There is little overall change in the structure of the enzyme between the N152A−moxalactam adduct and either the apo WT enzyme (*17*) or the WT−moxalactam structure (*19*) (C_α rmsd of 0.46 and 0.38 Å in monomer 2, respectively). Even in the active site, the positions of most key residues, such as Tyr150, Lys315, and Ala318, are highly conserved, with the only significant difference being observed in the side chain of Gln120, whose distal Nϵ moved by 1.6 Å relative to its position in the WT−moxalactam structure. We note that Gln120 is the most mobile of the conserved active site residues that we have observed in the approximately 20 AmpC structures that we have determined. The β-lactam carbonyl oxygen is in an almost identical location in the "electrophilic hole" (*13*, *17*, *38*), making polar interactions with backbone nitrogens of Ser64 and Ala318, just as in the WT−moxalactam adduct structure (*19*) (Figure 5). Interestingly, this is in contrast to the structure of the class A β-lactamase TEM-1 in complex with imipenem, in which the carbonyl oxygen is swung out of the electrophilic hole (*16*, *39*).

Despite only minor changes in the positions of the active site residues, the position of moxalactam within the active site changes significantly compared to the wild-type adduct (Table 3 and Figures 5 and 7). Consistent with the underlying hypothesis, the methoxy substituent of moxalactam found at the 7α position of the inhibitor is easily accommodated by the substituted Ala152 (Figure 6); there is no longer the steric overlap with Asn152 as seen in the WT−moxalactam structure (*19*). However, the absence of Asn152 has other consequences; there is no longer a chemical moiety that can interact with the carbonyl oxygen of the R_1 amide group (O10a) of moxalactam (see Table 3 for the numbering of moxalactam atoms). As a result, this R_1 carbonyl oxygen rotates 120°, leading to a 2.9 Å displacement relative to the WT complex with moxalactam (Figure 7). Instead of making polar interactions with both Gln120 Nϵ and Asn152 Nδ as it does in the WT complex, this carbonyl oxygen is only observed to hydrogen bond with an ordered water molecule

Table 3: Key Noncovalent Interactions Observed in the Crystal Structure of AmpC N152A in Complex with Moxalactam, Compared to Interactions Observed in the WT Complex

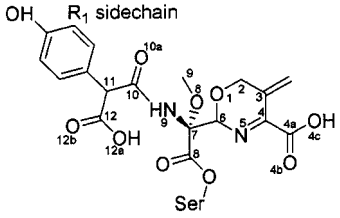

interaction	distance (Å)[a] in the N152A complex	distance (Å)[a,b] in the WT complex
S64 Oγ−K67 Nζ	2.8	2.7
K67 Nζ−Wat475	2.8	–
S64 Oγ−Y150 OH	2.9	2.8
Y150 OH−K315 Nζ	2.8	2.9
moxalactam O8−Wat475	2.8	–
moxalactam O4b−T316 Oγ	2.6	4.0
moxalactam O4b−Wat474	2.7	–
moxalactam O4c−Wat525/Wat402	2.4	2.7
moxalactam O4c−T316 Oγ	3.1	6.1
moxalactam β-lactam O−A318 N	2.9	3.0
moxalactam β-lactam O−A318 O	3.2	3.3
moxalactam β-lactam O−S64 N	2.9	2.9
moxalactam O10a−Wat475	2.8	–
moxalactam O12a−moxalactam N9	2.6	4.0
moxalactam O12b−Wat657	2.7	–
moxalactam O12b−Wat741	3.0	–

[a] All distances are for molecule 2 of the asymmetric unit. [b] From Patera et al. (*19*).

in the active site. Concomitantly, the hydrogen bond between the R_1 amide nitrogen (N9) of moxalactam and the backbone carbonyl oxygen of Ala318 is also disrupted in the N152A complex. The "tethering" that Asn152 (Asn132) provided to this carbonyl oxygen, and indeed to all β-lactams whose structures have been determined in complex with class C or class A β-lactamases (*13*, *14*, *19*, *20*, *38*, *40*), is apparently lost as a result of the residue substitution, which disrupts three hydrogen bonds between the ligand and the enzyme.

As a consequence of this rotation of the R_1 side chain of moxalactam, the oxacephem ring at the other end of the molecule has moved significantly (as much as 3.7 Å for a carboxylate oxygen), displacing the putative deacylating water from the position that it occupies in substrate (*19*) and transition-state analogue (*18*) complexes. The carboxylic acid

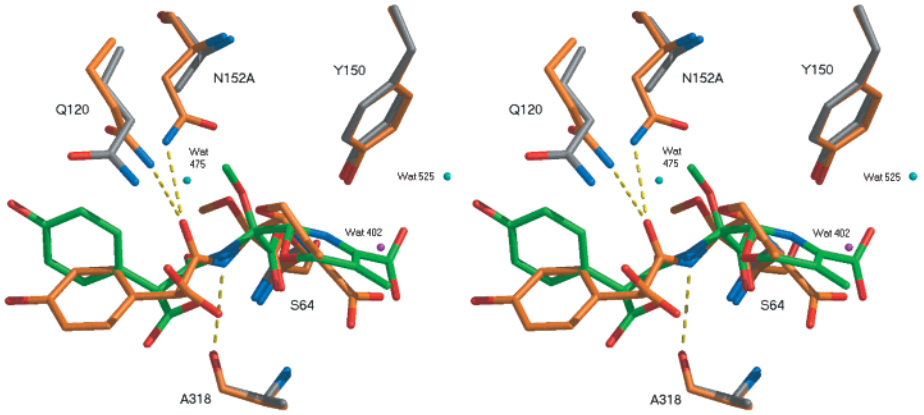

FIGURE 7: Stereoview of overlaid crystal structures of moxalactam in complex with WT AmpC (*19*) and with AmpC N152A. Atoms are colored as described in the legend of Figure 5, except carbon atoms in the WT structure are colored orange. The putative deacylating water (Wat402) in the WT structure is shown in magenta. The corresponding water (Wat525) in the N152A structure is shown in cyan. Dashed yellow lines represent key hydrogen bonds in the WT−moxalactam structure that are lost in the mutant structure. This figure was generated using MidasPlus (*52*).

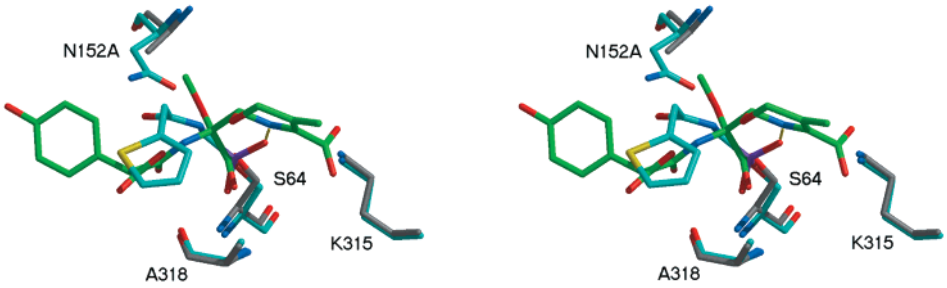

FIGURE 8: Stereoview of overlaid crystal structures of moxalactam in complex with AmpC N152A and a deacylation transition-state analogue (cephalothin acylglycine boronic acid) in complex with WT AmpC (*20*). Atoms are colored as described in the legend of Figure 5, except carbon atoms in the transition-state analogue structure are colored cyan, sulfur atoms yellow, and boron atoms purple. As shown by the dotted line, the oxacephem nitrogen of moxalactam is 1.4 Å from the O2 hydroxyl oxygen of the transition-state analogue, which represents the deacylating water. This figure was generated using MidasPlus (*52*).

of the oxacephem ring now occupies the position of the deacylating water (Figure 7) and interacts with Thr316 (Figure 5), a residue that formerly hydrogen bonded with this water (*19*). When the N152A−moxalactam complex is superimposed on a transition-state analogue complex with WT AmpC (*20*) (Figure 8), the ring nitrogen of the oxacephem (N5) is placed 1.4 Å from the transition-state analogue O2 hydroxyl. This oxygen represents the position of the deacylating water in the tetrahedral transition state of the deacylation step; the placement of the ring nitrogen thus blocks the formation of the transition state (*19*).

Overall, the N152A substitution appears to relieve the steric strain with the 7α-methoxy group of moxalactam. However, it also sacrifices key orienting interactions with the R_1 amide group of the ligand, resulting in a large rotation of the molecule into a conformation poorly suited to deacylation.

DISCUSSION

Moxalactam and imipenem destabilize AmpC when they form covalent adducts with the WT enzyme. Structural studies suggest that these 6(7)α-substituted β-lactams make unfavorable contacts with Asn152 and that these strained contacts are responsible for the reduction in enzyme stability and contribute to their ability to inhibit the enzyme. Such a hypothesis goes against our traditional view of inhibition involving complementary interactions and is an intriguing method of inhibition. To test this hypothesis, we substituted Asn152 with Ala in AmpC and measured the effects of moxalactam and imipenem on the stability of the mutant enzyme. The results of thermodynamic denaturation studies presented here are consistent with this hypothesis. Without Asn152, a significant portion of the strain introduced by the inhibitors has been eliminated: 1.10 kcal/mol in the case of moxalactam and 0.44 kcal/mol for imipenem (Table 1). Furthermore, in the crystal structure of the N152A−moxalactam complex, the unfavorable steric overlap between Asn152 and the 7α-methoxy substituent of moxalactam, observed in the WT−moxalactam complex, is eliminated (Figure 6).

When the widespread use of these antibiotics is considered, why have mutant β-lactamases containing substitutions of Asn152 not arisen in clinical isolates? It has long been known that Asn152 is a key catalytic residue (*24*); the k_{cat}/K_M value for N152A is reduced by more than 6300 times compared to that of WT AmpC. AmpC therefore finds itself in a Catch-22: although an unfavorable contact with Asn152 allows β-lactams with bulky 6(7)α substituents to inhibit the enzyme, AmpC cannot efficiently hydrolyze β-lactams without this residue.

The crystal structure of the N152A−moxalactam complex goes some way toward explaining this paradox. Without the hydrogen bond between Asn152 Nε and the carbonyl oxygen of moxalactam's R_1 side chain, the orientation of the R_1 group changes dramatically in the N152A complex compared to the WT complex with moxalactam and, indeed, from the

orientation adopted in a substrate complex (*19*) (Figure 7). This rotation of the R_1 group of moxalactam in turn shifts the oxacephem ring at the other end of the molecule (2.9 and 3.7 Å for each carboxylate oxygen, respectively), as though by a lever arm. Just as important, the ring nitrogen of the oxacephem is still only 1.4 Å away from where the tetrahedral, high-energy intermediate would form during the deacylation step of the hydrolysis reaction, as modeled by a boronic acid transition-state analogue (*20*). This would effectively prevent the formation of the transition state (Figure 8). This same inhibitory interaction was seen in the WT complex with moxalactam and contrasts with what was observed in the loracarbef substrate complex, where the analogous ring nitrogen was positioned to *stabilize* the formation of the high-energy tetrahedral intermediate (*19*). The rotation of the R_1 group also displaces the putative deacylating water, as an oxacephem carboxylate oxygen is now a mere 1.0 Å from the location of the deacylating water seen in the WT−moxalactam adduct. Thus, although Asn152 presents a steric barrier to 6(7)α substituents of β-lactams, the residue cannot be eliminated without doing substantial harm to the catalytic efficiency of class C β-lactamases.

Could a compromise between these conflicting demands emerge in the clinic? Perhaps, but our results suggest that simple point mutations in the active site are unlikely to be sufficient. In fact, imipenemases such as NMC-A (*8*) and IMI-1 (*41*) (both class A β-lactamases) have been found in clinical isolates of *Enterobacter cloacae* (*42*). The X-ray structure of NMC-A resembles that of TEM-1, but Asn132 (the residue analogous to Asn152 in AmpC) is shifted by 1.0 Å. It is interesting that this movement does not occur as a result of local changes in the active site, but rather is due to large-scale changes in structure throughout the enzyme. Although NMC-A and IMI-1 are 95% identical (*41*), comparison with other class A β-lactamases such as the SHV and TEM enzymes shows a level of sequence homology of only 40% with these more commonly encountered enzymes (*6*). Another chromosomal class A β-lactamase, SME-1, has emerged in *Serratia marcescens* isolates (*43*), showing carbapenemase activity, including resistance to imipenem (*44*, *45*). As with NMC-A, SME-1 also shows significant movement of Asn132 from what is typically seen in class A β-lactamases, a result of modifications in the enzyme far from the active site, including the introduction of a new disulfide bridge (*46*).

An artificial moxalactamase has been selected for using in vitro evolution by DNA shuffling of AmpC genes from four different species of bacterial pathogens. Here, too, the ability to hydrolyze moxalactam arose not through substitution of Asn152 but rather through swapping entire domains and stretches of amino acids, presumably allowing for the sort of active site reorganization seen in NMC-A (*47*).

A paradoxical feature of both imipenem and moxalactam is that these inhibitors are not highly complementary to their target enzymes, as would be expected of good noncovalent inhibitors; rather, they trap serine β-lactamases in a covalent adduct in which there are unfavorable contacts. These unfavorable contacts lead to a catalytically incompetent conformation of the β-lactam in the site, blocking deacylation (*19*). In this respect, moxalactam and imipenem resemble serpins, which also inhibit by distortion, albeit on a much larger scale. Like serpins, imipenem and moxalactam are spring-loaded for inhibition; the energy in this case is stored in the strained β-lactam bond itself. A lesson from moxalactam and imipenem is that better inhibitors may be designed not necessarily by optimizing complementary interactions but rather by engineering unfavorable, distorting contacts with key catalytic residues *within the covalent adduct*. Perversely, this mechanism of inhibition appears to leave these inhibitors less susceptible to the sort of point substitutions that have arisen in serine β-lactamases in response to other "β-lactamase resistant" β-lactams, such as clavulanate or the third-generation cephalosporins (*48*, *49*). Designing unfavorable interactions within scaffolds that form covalent adducts may be easier than designing favorable interactions, and β-lactams of this family (*50*) may merit further study.

ACKNOWLEDGMENT

We thank Rachel Powers, Pamela Focia, Douglas Freymann, and George Minasov for their advice and assistance with crystallographic methods. We thank Susan McGovern, Rachel Powers, and John Irwin for reading the manuscript. Crystallography data were collected at the DuPont-Northwestern-Dow Collaborative Access Team (DND-CAT) Synchrotron Research Center at the Advanced Photon Source. DND-CAT is supported by NSF Grant DMR-9304725 and the State of Illinois through Grant IBHE HECA NWU 96. Use of the Advanced Photon Source was supported by the U.S. Department of Energy under Contract W-31-102-Eng-38.

REFERENCES

1. Matagne, A., Dubus, A., Galleni, M., and Frere, J. M. (1999) *Nat. Prod. Rep. 16*, 1−19.
2. Neu, H. C. (1992) *Science 257*, 1064−73.
3. Davies, J. (1994) *Science 264*, 375−82.
4. Baquero, F., and Blazquez, J. (1997) *Trends Ecol. Evol. 11*, 482−7.
5. Fastrez, J., and Fersht, A. R. (1973) *Biochemistry 12*, 2025−34.
6. Naas, T., and Nordmann, P. (1994) *Proc. Natl. Acad. Sci. U.S.A. 91*, 7693−7.
7. Sougakoff, W., Jarlier, V., Delettre, J., Colloc'h, N., L'Hermite, G., Nordmann, P., and Naas, T. (1996) *J. Struct. Biol. 116*, 313−6.
8. Swaren, P., Maveyraud, L., Raquet, X., Cabantous, S., Duez, C., Pedelacq, J. D., Mariotte-Boyer, S., Mourey, L., Labia, R., Nicolas-Chanoine, M. H., Nordmann, P., Frere, J. M., and Samama, J. P. (1998) *J. Biol. Chem. 273*, 26714−21.
9. Tipper, D. J., and Strominger, J. L. (1965) *Proc. Natl. Acad. Sci. U.S.A. 54*, 1133−41.
10. Fisher, J., Belasco, J. G., Khosla, S., and Knowles, J. R. (1980) *Biochemistry 19*, 2895−901.
11. Easton, C. J., and Knowles, J. R. (1982) *Biochemistry 21*, 2857−62.
12. Herzberg, O., and Moult, J. (1987) *Science 236*, 694−701.
13. Oefner, C., D'Arcy, A., Daly, J. J., Gubernator, K., Charnas, R. L., Heinze, I., Hubschwerlen, C., and Winkler, F. K. (1990) *Nature 343*, 284−8.
14. Strynadka, N. C., Adachi, H., Jensen, S. E., Johns, K., Sielecki, A., Betzel, C., Sutoh, K., and James, M. N. (1992) *Nature 359*, 700−5.
15. Lobkovsky, E., Moews, P. C., Liu, H., Zhao, H., Frere, J. M., and Knox, J. R. (1993) *Proc. Natl. Acad. Sci. U.S.A. 90*, 11257−61.
16. Maveyraud, L., Mourey, L., Kotra, L. P., Pedelacq, J., Guillet, V., Mobashery, S., and Samama, J. (1998) *J. Am. Chem. Soc. 120*, 9748−52.

17. Usher, K. C., Blaszczak, L. C., Weston, G. S., Shoichet, B. K., and Remington, S. J. (1998) *Biochemistry 37*, 16082−92.
18. Powers, R. A., Blazquez, J., Weston, G. S., Morosini, M. I., Baquero, F., and Shoichet, B. K. (1999) *Protein Sci. 8*, 2330−7.
19. Patera, A., Blaszczak, L. C., and Shoichet, B. K. (2000) *J. Am. Chem. Soc. 122*, 10504−12.
20. Caselli, E., Powers, R. A., Blaszczak, L. C., Wu, C. Y. E., Prati, F., and Shoichet, B. K. (2001) *Chem. Biol. 8*, 17−31.
21. Matagne, A., Lamotte-Brasseur, J., Dive, G., Knox, J. R., and Frere, J. M. (1993) *Biochem. J. 293*, 607−11.
22. Beadle, B. M., McGovern, S. L., Patera, A., and Shoichet, B. K. (1999) *Protein Sci. 8*, 1816−24.
23. Massova, I., and Mobashery, S. (1998) *Antimicrob. Agents Chemother. 42*, 1−17.
24. Dubus, A., Normark, S., Kania, M., and Page, M. G. (1995) *Biochemistry 34*, 7757−64.
25. Jacob, F., Joris, B., Lepage, S., Dusart, J., and Frere, J. M. (1990) *Biochem. J. 271*, 399−406.
26. Ho, S. N., Hunt, H. D., Horton, R. M., Pullen, J. K., and Pease, L. R. (1989) *Gene 77*, 51−9.
27. Kirchhoff, W. (1993) National Institute of Standards and Technology, Gaithersburg, MD.
28. Raquet, X., Lamotte-Brasseur, J., Fonze, E., Goussard, S., Courvalin, P., and Frere, J. M. (1994) *J. Mol. Biol. 244*, 625−39.
29. Becktel, W. J., and Schellman, J. A. (1987) *Biopolymers 26*, 1859−77.
30. Matagne, A., Misselyn-Bauduin, A. M., Joris, B., Erpicum, T., Granier, B., and Frere, J. M. (1990) *Biochem. J. 265*, 131−46.
31. Page, M. G. (1993) *Biochem. J. 295*, 295−304.
32. Dryjanski, M., and Pratt, R. F. (1995) *Biochemistry 34*, 3561−8.
33. Weston, G. S., Blazquez, J., Baquero, F., and Shoichet, B. K. (1998) *J. Med. Chem. 41*, 4577−86.
34. Otwinowski, Z., and Minor, W. (1997) *Methods Enzymol. 276*, 307−26.
35. Brunger, A. T., Adams, P. D., Clore, G. M., DeLano, W. L., Gros, P., Grosse-Kunstleve, R. W., Jiang, J. S., Kuszewski, J., Nilges, M., Pannu, N. S., Read, R. J., Rice, L. M., Simonson, T., and Warren, G. L. (1998) *Acta Crystallogr. D54*, 905−21.
36. Jones, T. A., Zou, J. Y., Cowan, S. W., and Kjeldgaard, M. (1991) *Acta Crystallogr. A47*, 110−9.
37. Laskowski, R. A., MacArthur, M. W., Moss, D. S., and Thornton, J. M. (1993) *J. Appl. Crystallogr. 26*, 283−91.
38. Lobkovsky, E., Billings, E. M., Moews, P. C., Rahil, J., Pratt, R. F., and Knox, J. R. (1994) *Biochemistry 33*, 6762−72.
39. Swaren, P., Massova, I., Bellettini, J. R., Bulychev, A., Maveyraud, L., Kotra, L. P., Miller, M. J., Mobashery, S., and Samama, J. P. (1999) *J. Am. Chem. Soc. 121*, 5353−9.
40. Chen, C. C. H., and Herzberg, O. (2001) *Biochemistry 40*, 2351−8.
41. Rasmussen, B. A., Bush, K., Keeney, D., Yang, Y., Hare, R., O'Gara, C., and Medeiros, A. A. (1996) *Antimicrob. Agents Chemother. 40*, 2080−6.
42. Rasmussen, B. A., and Bush, K. (1997) *Antimicrob. Agents Chemother. 41*, 223−32.
43. Naas, T., Vandel, L., Sougakoff, W., Livermore, D. M., and Nordmann, P. (1994) *Antimicrob. Agents Chemother. 38*, 1262−70.
44. Nordmann, P. (1998) *Clin. Infect. Dis. 27* (Suppl. 1), S100−6.
45. Queenan, A. M., Torres-Viera, C., Gold, H. S., Carmeli, Y., Eliopoulos, G. M., Moellering, R. C., Jr., Quinn, J. P., Hindler, J., Medeiros, A. A., and Bush, K. (2000) *Antimicrob. Agents Chemother. 44*, 3035−9.
46. Raquet, X., Lamotte-Brasseur, J., Bouillenne, F., and Frere, J. M. (1997) *Proteins 27*, 47−58.
47. Crameri, A., Raillard, S. A., Bermudez, E., and Stemmer, W. P. (1998) *Nature 391*, 288−91.
48. Vakulenko, S. B., Taibi-Tronche, P., Toth, M., Massova, I., Lerner, S. A., and Mobashery, S. (1999) *J. Biol. Chem. 274*, 23052−60.
49. Swaren, P., Golemi, D., Cabantous, S., Bulychev, A., Maveyraud, L., Mobashery, S., and Samama, J. P. (1999) *Biochemistry 38*, 9570−6.
50. Maveyraud, L., Massova, I., Birck, W., Miyashita, K., Samama, J. P., and Mobashery, S. (1996) *J. Am. Chem. Soc. 118*, 7435−40.
51. Evans, S. V. (1993) *J. Mol. Graphics 11*, 134−8, 127−8.
52. Ferrin, T. E., Huang, C. C., Jarvis, L. E., and Langridge, R. (1988) *J. Mol. Graphics 6*, 13−27.

BI010641M